Search for the Standard Model Higgs Boson in the $H \to WW \to \ell\nu q'\bar{q}$ Decay Channel

V.M. Abazov,[35] B. Abbott,[72] B.S. Acharya,[29] M. Adams,[48] T. Adams,[46] G.D. Alexeev,[35] G. Alkhazov,[39] A. Alton[a],[60] G. Alverson,[59] G.A. Alves,[2] L.S. Ancu,[34] M. Aoki,[47] M. Arov,[57] A. Askew,[46] B. Åsman,[40] O. Atramentov,[64] C. Avila,[8] J. BackusMayes,[79] F. Badaud,[13] L. Bagby,[47] B. Baldin,[47] D.V. Bandurin,[46] S. Banerjee,[29] E. Barberis,[59] P. Baringer,[55] J. Barreto,[3] J.F. Bartlett,[47] U. Bassler,[18] V. Bazterra,[48] S. Beale,[6] A. Bean,[55] M. Begalli,[3] M. Begel,[70] C. Belanger-Champagne,[40] L. Bellantoni,[47] S.B. Beri,[27] G. Bernardi,[17] R. Bernhard,[22] I. Bertram,[41] M. Besançon,[18] R. Beuselinck,[42] V.A. Bezzubov,[38] P.C. Bhat,[47] V. Bhatnagar,[27] G. Blazey,[49] S. Blessing,[46] K. Bloom,[63] A. Boehnlein,[47] D. Boline,[69] T.A. Bolton,[56] E.E. Boos,[37] G. Borissov,[41] T. Bose,[58] A. Brandt,[75] O. Brandt,[23] R. Brock,[61] G. Brooijmans,[67] A. Bross,[47] D. Brown,[17] J. Brown,[17] X.B. Bu,[47] M. Buehler,[78] V. Buescher,[24] V. Bunichev,[37] S. Burdin[b],[41] T.H. Burnett,[79] C.P. Buszello,[40] B. Calpas,[15] E. Camacho-Pérez,[32] M.A. Carrasco-Lizarraga,[55] B.C.K. Casey,[47] H. Castilla-Valdez,[32] S. Chakrabarti,[69] D. Chakraborty,[49] K.M. Chan,[53] A. Chandra,[77] G. Chen,[55] S. Chevalier-Théry,[18] D.K. Cho,[74] S.W. Cho,[31] S. Choi,[31] B. Choudhary,[28] T. Christoudias,[42] S. Cihangir,[47] D. Claes,[63] J. Clutter,[55] M. Cooke,[47] W.E. Cooper,[47] M. Corcoran,[77] F. Couderc,[18] M.-C. Cousinou,[15] A. Croc,[18] D. Cutts,[74] A. Das,[44] G. Davies,[42] K. De,[75] S.J. de Jong,[34] E. De La Cruz-Burelo,[32] F. Déliot,[18] M. Demarteau,[47] R. Demina,[68] D. Denisov,[47] S.P. Denisov,[38] S. Desai,[47] K. DeVaughan,[63] H.T. Diehl,[47] M. Diesburg,[47] A. Dominguez,[63] T. Dorland,[79] A. Dubey,[28] L.V. Dudko,[37] D. Duggan,[64] A. Duperrin,[15] S. Dutt,[27] A. Dyshkant,[49] M. Eads,[63] D. Edmunds,[61] J. Ellison,[45] V.D. Elvira,[47] Y. Enari,[17] H. Evans,[51] A. Evdokimov,[70] V.N. Evdokimov,[38] G. Facini,[59] T. Ferbel,[68] F. Fiedler,[24] F. Filthaut,[34] W. Fisher,[61] H.E. Fisk,[47] M. Fortner,[49] H. Fox,[41] S. Fuess,[47] T. Gadfort,[70] A. Garcia-Bellido,[68] V. Gavrilov,[36] P. Gay,[13] W. Geist,[19] W. Geng,[15, 61] D. Gerbaudo,[65] C.E. Gerber,[48] Y. Gershtein,[64] G. Ginther,[47, 68] G. Golovanov,[35] A. Goussiou,[79] P.D. Grannis,[69] S. Greder,[19] H. Greenlee,[47] Z.D. Greenwood,[57] E.M. Gregores,[4] G. Grenier,[20] Ph. Gris,[13] J.-F. Grivaz,[16] A. Grohsjean,[18] S. Grünendahl,[47] M.W. Grünewald,[30] F. Guo,[69] G. Gutierrez,[47] P. Gutierrez,[72] A. Haas[c],[67] S. Hagopian,[46] J. Haley,[59] L. Han,[7] K. Harder,[43] A. Harel,[68] J.M. Hauptman,[54] J. Hays,[42] T. Head,[43] T. Hebbeker,[21] D. Hedin,[49] H. Hegab,[73] A.P. Heinson,[45] U. Heintz,[74] C. Hensel,[23] I. Heredia-De La Cruz,[32] K. Herner,[60] M.D. Hildreth,[53] R. Hirosky,[78] T. Hoang,[46] J.D. Hobbs,[69] B. Hoeneisen,[12] M. Hohlfeld,[24] S. Hossain,[72] Z. Hubacek,[10, 18] N. Huske,[17] V. Hynek,[10] I. Iashvili,[66] R. Illingworth,[47] A.S. Ito,[47] S. Jabeen,[74] M. Jaffré,[16] S. Jain,[66] D. Jamin,[15] R. Jesik,[42] K. Johns,[44] M. Johnson,[47] D. Johnston,[63] A. Jonckheere,[47] P. Jonsson,[42] J. Joshi,[27] A. Juste[d],[47] K. Kaadze,[56] E. Kajfasz,[15] D. Karmanov,[37] P.A. Kasper,[47] I. Katsanos,[63] R. Kehoe,[76] S. Kermiche,[15] N. Khalatyan,[47] A. Khanov,[73] A. Kharchilava,[66] Y.N. Kharzheev,[35] D. Khatidze,[74] M.H. Kirby,[50] J.M. Kohli,[27] A.V. Kozelov,[38] J. Kraus,[61] A. Kumar,[66] A. Kupco,[11] T. Kurča,[20] V.A. Kuzmin,[37] J. Kvita,[9] S. Lammers,[51] G. Landsberg,[74] P. Lebrun,[20] H.S. Lee,[31] S.W. Lee,[54] W.M. Lee,[47] J. Lellouch,[17] L. Li,[45] Q.Z. Li,[47] S.M. Lietti,[5] J.K. Lim,[31] D. Lincoln,[47] J. Linnemann,[61] V.V. Lipaev,[38] R. Lipton,[47] Y. Liu,[7] Z. Liu,[6] A. Lobodenko,[39] M. Lokajicek,[11] P. Love,[41] H.J. Lubatti,[79] R. Luna-Garcia[e],[32] A.L. Lyon,[47] A.K.A. Maciel,[2] D. Mackin,[77] R. Madar,[18] R. Magaña-Villalba,[32] S. Malik,[63] V.L. Malyshev,[35] Y. Maravin,[56] J. Martínez-Ortega,[32] R. McCarthy,[69] C.L. McGivern,[55] M.M. Meijer,[34] A. Melnitchouk,[62] D. Menezes,[49] P.G. Mercadante,[4] M. Merkin,[37] A. Meyer,[21] J. Meyer,[23] F. Miconi,[19] N.K. Mondal,[29] G.S. Muanza,[15] M. Mulhearn,[78] E. Nagy,[15] M. Naimuddin,[28] M. Narain,[74] R. Nayyar,[28] H.A. Neal,[60] J.P. Negret,[8] P. Neustroev,[39] S.F. Novaes,[5] T. Nunnemann,[25] G. Obrant,[39] J. Orduna,[32] N. Osman,[42] J. Osta,[53] G.J. Otero y Garzón,[1] M. Owen,[43] M. Padilla,[45] M. Pangilinan,[74] N. Parashar,[52] V. Parihar,[74] S.K. Park,[31] J. Parsons,[67] R. Partridge[c],[74] N. Parua,[51] A. Patwa,[70] B. Penning,[47] M. Perfilov,[37] K. Peters,[43] Y. Peters,[43] G. Petrillo,[68] P. Pétroff,[16] R. Piegaia,[1] J. Piper,[61] M.-A. Pleier,[70] P.L.M. Podesta-Lerma[f],[32] V.M. Podstavkov,[47] M.-E. Pol,[2] P. Polozov,[36] A.V. Popov,[38] M. Prewitt,[77] D. Price,[51] S. Protopopescu,[70] J. Qian,[60] A. Quadt,[23] B. Quinn,[62] M.S. Rangel,[2] K. Ranjan,[28] P.N. Ratoff,[41] I. Razumov,[38] P. Renkel,[76] M. Rijssenbeek,[69] I. Ripp-Baudot,[19] F. Rizatdinova,[73] M. Rominsky,[47] C. Royon,[18] P. Rubinov,[47] R. Ruchti,[53] G. Safronov,[36] G. Sajot,[14] A. Sánchez-Hernández,[32] M.P. Sanders,[25] B. Sanghi,[47] A.S. Santos,[5] G. Savage,[47] L. Sawyer,[57] T. Scanlon,[42] R.D. Schamberger,[69] Y. Scheglov,[39] H. Schellman,[50] T. Schliephake,[26] S. Schlobohm,[79] C. Schwanenberger,[43] R. Schwienhorst,[61] J. Sekaric,[55] H. Severini,[72] E. Shabalina,[23] V. Shary,[18] A.A. Shchukin,[38] R.K. Shivpuri,[28] V. Simak,[10] V. Sirotenko,[47] P. Skubic,[72] P. Slattery,[68] D. Smirnov,[53] K.J. Smith,[66] G.R. Snow,[63]

J. Snow,[71] S. Snyder,[70] S. Söldner-Rembold,[43] L. Sonnenschein,[21] A. Sopczak,[41] M. Sosebee,[75] K. Soustruznik,[9] B. Spurlock,[75] J. Stark,[14] V. Stolin,[36] D.A. Stoyanova,[38] M. Strauss,[72] D. Strom,[48] L. Stutte,[47] L. Suter,[43] P. Svoisky,[72] M. Takahashi,[43] A. Tanasijczuk,[1] W. Taylor,[6] M. Titov,[18] V.V. Tokmenin,[35] Y.-T. Tsai,[68] D. Tsybychev,[69] B. Tuchming,[18] C. Tully,[65] P.M. Tuts,[67] L. Uvarov,[39] S. Uvarov,[39] S. Uzunyan,[49] R. Van Kooten,[51] W.M. van Leeuwen,[33] N. Varelas,[48] E.W. Varnes,[44] I.A. Vasilyev,[38] P. Verdier,[20] L.S. Vertogradov,[35] M. Verzocchi,[47] M. Vesterinen,[43] D. Vilanova,[18] P. Vint,[42] P. Vokac,[10] H.D. Wahl,[46] M.H.L.S. Wang,[68] J. Warchol,[53] G. Watts,[79] M. Wayne,[53] M. Weber,[g,47] L. Welty-Rieger,[50] A. White,[75] D. Wicke,[26] M.R.J. Williams,[41] G.W. Wilson,[55] S.J. Wimpenny,[45] M. Wobisch,[57] D.R. Wood,[59] T.R. Wyatt,[43] Y. Xie,[47] C. Xu,[60] S. Yacoob,[50] R. Yamada,[47] W.-C. Yang,[43] T. Yasuda,[47] Y.A. Yatsunenko,[35] Z. Ye,[47] H. Yin,[47] K. Yip,[70] S.W. Youn,[47] J. Yu,[75] S. Zelitch,[78] T. Zhao,[79] B. Zhou,[60] J. Zhu,[60] M. Zielinski,[68] D. Zieminska,[51] and L. Zivkovic[74]

(The D0 Collaboration[∗])

[1]*Universidad de Buenos Aires, Buenos Aires, Argentina*
[2]*LAFEX, Centro Brasileiro de Pesquisas Físicas, Rio de Janeiro, Brazil*
[3]*Universidade do Estado do Rio de Janeiro, Rio de Janeiro, Brazil*
[4]*Universidade Federal do ABC, Santo André, Brazil*
[5]*Instituto de Física Teórica, Universidade Estadual Paulista, São Paulo, Brazil*
[6]*Simon Fraser University, Vancouver, British Columbia, and York University, Toronto, Ontario, Canada*
[7]*University of Science and Technology of China, Hefei, People's Republic of China*
[8]*Universidad de los Andes, Bogotá, Colombia*
[9]*Charles University, Faculty of Mathematics and Physics,*
Center for Particle Physics, Prague, Czech Republic
[10]*Czech Technical University in Prague, Prague, Czech Republic*
[11]*Center for Particle Physics, Institute of Physics,*
Academy of Sciences of the Czech Republic, Prague, Czech Republic
[12]*Universidad San Francisco de Quito, Quito, Ecuador*
[13]*LPC, Université Blaise Pascal, CNRS/IN2P3, Clermont, France*
[14]*LPSC, Université Joseph Fourier Grenoble 1, CNRS/IN2P3,*
Institut National Polytechnique de Grenoble, Grenoble, France
[15]*CPPM, Aix-Marseille Université, CNRS/IN2P3, Marseille, France*
[16]*LAL, Université Paris-Sud, CNRS/IN2P3, Orsay, France*
[17]*LPNHE, Universités Paris VI and VII, CNRS/IN2P3, Paris, France*
[18]*CEA, Irfu, SPP, Saclay, France*
[19]*IPHC, Université de Strasbourg, CNRS/IN2P3, Strasbourg, France*
[20]*IPNL, Université Lyon 1, CNRS/IN2P3, Villeurbanne, France and Université de Lyon, Lyon, France*
[21]*III. Physikalisches Institut A, RWTH Aachen University, Aachen, Germany*
[22]*Physikalisches Institut, Universität Freiburg, Freiburg, Germany*
[23]*II. Physikalisches Institut, Georg-August-Universität Göttingen, Göttingen, Germany*
[24]*Institut für Physik, Universität Mainz, Mainz, Germany*
[25]*Ludwig-Maximilians-Universität München, München, Germany*
[26]*Fachbereich Physik, Bergische Universität Wuppertal, Wuppertal, Germany*
[27]*Panjab University, Chandigarh, India*
[28]*Delhi University, Delhi, India*
[29]*Tata Institute of Fundamental Research, Mumbai, India*
[30]*University College Dublin, Dublin, Ireland*
[31]*Korea Detector Laboratory, Korea University, Seoul, Korea*
[32]*CINVESTAV, Mexico City, Mexico*
[33]*FOM-Institute NIKHEF and University of Amsterdam/NIKHEF, Amsterdam, The Netherlands*
[34]*Radboud University Nijmegen/NIKHEF, Nijmegen, The Netherlands*
[35]*Joint Institute for Nuclear Research, Dubna, Russia*
[36]*Institute for Theoretical and Experimental Physics, Moscow, Russia*
[37]*Moscow State University, Moscow, Russia*
[38]*Institute for High Energy Physics, Protvino, Russia*
[39]*Petersburg Nuclear Physics Institute, St. Petersburg, Russia*
[40]*Stockholm University, Stockholm and Uppsala University, Uppsala, Sweden*
[41]*Lancaster University, Lancaster LA1 4YB, United Kingdom*
[42]*Imperial College London, London SW7 2AZ, United Kingdom*
[43]*The University of Manchester, Manchester M13 9PL, United Kingdom*
[44]*University of Arizona, Tucson, Arizona 85721, USA*
[45]*University of California Riverside, Riverside, California 92521, USA*
[46]*Florida State University, Tallahassee, Florida 32306, USA*
[47]*Fermi National Accelerator Laboratory, Batavia, Illinois 60510, USA*

^{48}University of Illinois at Chicago, Chicago, Illinois 60607, USA
^{49}Northern Illinois University, DeKalb, Illinois 60115, USA
^{50}Northwestern University, Evanston, Illinois 60208, USA
^{51}Indiana University, Bloomington, Indiana 47405, USA
^{52}Purdue University Calumet, Hammond, Indiana 46323, USA
^{53}University of Notre Dame, Notre Dame, Indiana 46556, USA
^{54}Iowa State University, Ames, Iowa 50011, USA
^{55}University of Kansas, Lawrence, Kansas 66045, USA
^{56}Kansas State University, Manhattan, Kansas 66506, USA
^{57}Louisiana Tech University, Ruston, Louisiana 71272, USA
^{58}Boston University, Boston, Massachusetts 02215, USA
^{59}Northeastern University, Boston, Massachusetts 02115, USA
^{60}University of Michigan, Ann Arbor, Michigan 48109, USA
^{61}Michigan State University, East Lansing, Michigan 48824, USA
^{62}University of Mississippi, University, Mississippi 38677, USA
^{63}University of Nebraska, Lincoln, Nebraska 68588, USA
^{64}Rutgers University, Piscataway, New Jersey 08855, USA
^{65}Princeton University, Princeton, New Jersey 08544, USA
^{66}State University of New York, Buffalo, New York 14260, USA
^{67}Columbia University, New York, New York 10027, USA
^{68}University of Rochester, Rochester, New York 14627, USA
^{69}State University of New York, Stony Brook, New York 11794, USA
^{70}Brookhaven National Laboratory, Upton, New York 11973, USA
^{71}Langston University, Langston, Oklahoma 73050, USA
^{72}University of Oklahoma, Norman, Oklahoma 73019, USA
^{73}Oklahoma State University, Stillwater, Oklahoma 74078, USA
^{74}Brown University, Providence, Rhode Island 02912, USA
^{75}University of Texas, Arlington, Texas 76019, USA
^{76}Southern Methodist University, Dallas, Texas 75275, USA
^{77}Rice University, Houston, Texas 77005, USA
^{78}University of Virginia, Charlottesville, Virginia 22901, USA
^{79}University of Washington, Seattle, Washington 98195, USA
(Dated: January 29, 2011)

We present a search for the standard model Higgs boson (H) in $p\bar{p}$ collisions at $\sqrt{s} = 1.96$ TeV in events containing a charged lepton (ℓ), missing transverse energy, and at least two jets, using 5.4 fb^{-1} of integrated luminosity recorded with the D0 detector at the Fermilab Tevatron Collider. This analysis is sensitive primarily to Higgs bosons produced through the fusion of two gluons or two electroweak bosons, with subsequent decay $H \to WW \to \ell\nu q'\bar{q}$, where ℓ is an electron or muon. The search is also sensitive to contributions from other production channels, such as $WH \to \ell\nu b\bar{b}$. In the absence of signal, we set limits at the 95% C.L. on the cross section for H production $\sigma(p\bar{p} \to H + X)$ in these final states. For a mass of $M_H = 160$ GeV, the limit is a factor of 3.9 larger than the cross section in the standard model, and consistent with expectation.

The Higgs mechanism [1–4] accommodates the observed breaking of electroweak (EW) symmetry in the standard model (SM). In addition to generating masses for the EW W and Z bosons, as well as for fermions, the theory predicts a new scalar Higgs boson (H) with well-determined couplings, but unknown mass (M_H). Confirmation of the existence and properties of the H boson would be a key step in elucidating the origins of EW symmetry breaking. For a Higgs boson with mass $M_H \gtrsim 135$ GeV, the dominant decay mode is $H \to W^+W^-$, where at least one W boson must be virtual when $M_H < 2M_W$. Previous searches [5–7] for this process were based on events with two charged leptons (ℓ) and large missing transverse energy ($\not{E}_T$) from the decay $H \to W^+W^- \to \bar{\ell}\nu\ell'\bar{\nu}'$ ($\ell = e, \mu$). This Letter presents the first search for production of Higgs bosons with subsequent decay to WW having only one charged lepton in the final state. The data sample is 5.4 fb^{-1} of integrated luminosity in $p\bar{p}$ collisions at $\sqrt{s} = 1.96$ TeV recorded with the D0 detector at the Fermilab Tevatron Collider. The largest SM contributions to the inclusive cross section for producing H bosons in $p\bar{p}$ collisions are

*with visitors from ^{a}Augustana College, Sioux Falls, SD, USA, ^{b}The University of Liverpool, Liverpool, UK, ^{c}SLAC, Menlo Park, CA, USA, ^{d}ICREA/IFAE, Barcelona, Spain, ^{e}Centro de Investigacion en Computacion - IPN, Mexico City, Mexico, ^{f}ECFM, Universidad Autonoma de Sinaloa, Culiacán, Mexico, and ^{g}Universität Bern, Bern, Switzerland.

from mechanisms involving the fusion of two gluons or two weak vector bosons into an H boson, and associated production of H and a weak vector boson ($V = W$ or Z). In the following we will not distinguish between particles and antiparticles. The most striking signatures from $H \to VV$ decays are in the purely leptonic final states, but these account for only 5% of such decays. Final states containing a single charged lepton have larger backgrounds, but their branching fractions are a factor of ≈ 6 larger than for the all-leptonic modes.

A recent calculation of the differential width for $H \to WW \to \ell\nu q'q$ decays [8] supports the important role of these mixed modes for characterizing a potential SM Higgs-boson signal. Our analysis is most sensitive to final-state topologies with a single lepton (e or μ), two or more jets, and E_T, arising from $H \to WW \to \ell\nu q'q$ decays. For $M_H \lesssim 140\,\text{GeV}$, significant sensitivity is gained from $WH \to \ell\nu bb$, where we do not attempt to identify the b quark flavor. Smaller signal contributions from $H \to ZZ \to \ell\ell qq$, where ℓ represents an unidentified lepton, and $H \to WW \to \tau\nu q'q$ with $\tau \to \ell\nu\nu$ are also included. For $M_H \geq 160\,\text{GeV}$, assuming that the observed E_T is due to the neutrino from the decay of a W boson, it is possible to reconstruct the longitudinal momentum (p_z^ν) up to a twofold ambiguity, and thereby extract the mass of the H decaying to WW [9]. We choose the solution with smallest $|\text{Re}(p_z^\nu)|$ to calculate M_H. The primary backgrounds are from V+jets, top quark, diboson production, and multijet (MJ) events containing a lepton or lepton-like signature with E_T generally arising from mismeasurement of jet energies.

The D0 detector [10] consists of tracking, calorimetric and muon detectors. Charged particle tracks are reconstructed using silicon microstrip (SMT) detectors and a scintillating fiber tracker, within a 2 T solenoid. Three uranium/liquid-argon calorimeters measure particle energies that are reconstructed into hadronic jets using an iterative midpoint cone algorithm with a cone radius of 0.5 [11]. Electrons and muons are identified through association of charged particle tracks with clusters in the electromagnetic sections of the calorimeters or with hits in the muon detector, respectively. We obtain the E_T from a vector sum of transverse components of calorimeter energy depositions and correct it for identified muons. Jet energies are calibrated using transverse momentum balance in photon+jet events [12], and the correction is propagated to the E_T. The data are recorded using triggers designed to select single electrons or muons and combination of electron and jets. After imposing data quality requirements, the total integrated luminosity is $5.4\,\text{fb}^{-1}$ [13], where the first $1.1\,\text{fb}^{-1}$, Run IIa, precedes an upgrade to the SMT and trigger systems. The remaining $4.3\,\text{fb}^{-1}$ is denoted as Run IIb. The four data sets using e or μ for the two run epochs are analyzed separately and combined in the final result.

Background contributions from most SM processes are determined through Monte Carlo (MC) simulation, while multijet background is estimated from data. The dominant background is from V+jets processes, which are generated with ALPGEN [14]. The transverse momentum (p_T) spectrum of the Z boson in the MC is reweighted to match that observed in data [15]. The p_T spectrum of the W boson is reweighted using the same dependence, but corrected for differences between the p_T spectra of Z and W bosons predicted in next-to-next-to-leading order (NNLO) QCD [16]. Backgrounds from $t\bar{t}$ and electroweak single top quark production are simulated using the ALPGEN and COMPHEP [17] generators, respectively. Vector boson pair production and H boson signals are generated with PYTHIA [18]. All these simulations use CTEQ6L1 parton distribution functions (PDF) [19]. Both ALPGEN and COMPHEP samples are interfaced with PYTHIA for modeling of parton evolution and hadronization.

Relative normalizations for the various V+jets processes are obtained from calculations of cross sections at next-to-leading order using MCFM [20], while the absolute normalization for the total V+jets background is constrained through a comparison to data, following the subtraction of other background sources. This increases the normalization for V+jets background by about 2%, compared with the expectation from ALPGEN normalized using total cross sections calculated at NNLO [21] with the MRST2004 NNLO PDFs [22]. Cross sections for other SM backgrounds are taken from Ref. [23], or calculated with MCFM, and those for signal are taken from Ref. [24]. The p_T spectra for diboson events in background are corrected to match those of the MC@NLO generator [25]. The p_T spectra from the contribution of gluon fusion to the H boson signal, generated in PYTHIA, are modified to match those obtained from SHERPA [26].

Signal and background events from MC are passed through a full GEANT3-based simulation [27] of detector response, then processed with the same reconstruction program as used for data. Events from randomly selected beam crossings with the same instantaneous luminosity profile as data are overlaid on the simulated events to model detector noise and contributions from the presence of additional $p\bar{p}$ interactions. Parameterizations of trigger efficiency for leptons are determined using $Z \to \ell\ell$ decays [28]. Any remaining differences between data and simulation in the reconstruction of electrons, muons, and jets are adjusted in simulated events to match those observed in data and these corrections are propagated to the MET.

Events are selected to contain candidates for $W \to \ell\nu$ decay by requiring $E_T > 15\,\text{GeV}$ and the presence of a lepton with $p_T > 15\,\text{GeV}$ that is isolated relative to jets, namely located outside jet cones $\Delta R(\ell, j) > 0.5$, with $(\Delta R)^2 = (\phi^\ell - \phi^j)^2 + (\eta^\ell - \eta^j)^2$, where ϕ^x and η^x are the azimuth and pseudorapidity [29] of object x. The $p\bar{p}$ interaction vertex (PV) position along the beam

TABLE I: Number of signal and background events expected after selection requirements. The signal sources include gluon-gluon and vector-boson fusion, and associated production WH. The three numbers quoted for the signals correspond to $M_H = 130, 160,$ and $190\,\text{GeV}$. For backgrounds, "top" includes pair and single top quark production and "VV" includes all non-signal diboson processes. The overall background normalization is fixed to the data by adjusting the V+jets cross sections.

Channel	$gg \rightarrow H$	$qq \rightarrow qqH$	WH	V+jets	Multijet	Top	VV	Total Background	Data
Electron	11.2/46.3/27.8	2.1/6.4/4.2	7.2/0/0	52158	11453	2433	1584	67627	67627
Muon	9.5/34.7/20.4	1.5/4.4/2.9	5.7/0/0	47970	2720	1598	1273	53562	53562

direction (z_{PV}) is required to be reconstructed within the longitudinal acceptance of the SMT, $|z_{\text{PV}}| < 60$ cm. The lepton is required to originate from the PV and to pass more restrictive isolation criteria based on tracking information and energy deposited near the lepton in the calorimeter. Electrons must also satisfy criteria for the spatial distribution of the shower, and timing information is used to reject cosmic ray background in events with muons. All lepton selections are described in Ref. [30], except that this analysis requires both the scalar sum of track p_T and calorimeter energy in the vicinity of the muon be less than $2.5\,\text{GeV}$. Electrons and muons are required to be located within $|\eta_{\text{det}}| < 1.1$ and < 1.6, respectively, where η_{det} is the pseudorapidity assuming the object originates from the center of the detector. To reduce background from $Z \rightarrow \ell\ell$, top quark, and diboson events, and to assure selected events do not overlap with those used in the $WW \rightarrow \ell\nu\ell'\nu'$ analysis channels, we veto any event containing an additional lepton satisfying less stringent identification criteria. We also require at least two jets with $|\eta^j| < 2.5$ and $p_T > 20\,\text{GeV}$ that contain associated tracks originating from the PV. The jet p_T requirement is $23\,\text{GeV}$ when the second-leading jet (ordered in p_T) has $0.8 < |\eta_{det}| < 1.5$ [10]. The leading two jets are used to reconstruct the W boson decaying to $q'q$. To suppress background from MJ events [31], we require events to have $M_T^W (\text{GeV}) > 40 - 0.5 \times \not{E}_T$, where M_T^W is the transverse mass [32] of the W boson candidate.

To estimate the MJ background, we use data samples orthogonal to our signal sample. For the electron channel, we form a "loose" category for which the selection on a likelihood discriminant used to select a "tight" electron, based on calorimeter and track variables [31], is reversed. Following the method of Ref. [33], the MJ background is evaluated from independently-determined probabilities for loose electrons or jets to pass the tight signal selections. For the muon channel, we reverse requirements on muon isolation in both the tracking detectors and the calorimeters, and subtract contributions arising from SM processes containing a true muon from W or Z decay. The normalization is obtained from fits to both the V+jets and MJ contributions using observed distributions of p_T^μ and $\not{E}_T$. Event yields in data and those expected for signal and background are shown in Table I.

We use a random forest (RF) of 50 decision trees (DT) to separate signal from background [34, 35]. Each DT is trained on a randomly selected collection of signal and background MC events as well as MJ events from data. The DTs examine a random set of about 30 discriminating variables formed from particle 4-vectors, angles between objects, and combinations of kinematic variables such as reconstructed masses and event shapes. An RF is trained separately for each data set, using signal hypotheses $115 < M_H < 200\,\text{GeV}$ in steps of $5\,\text{GeV}$. The outputs of the final RF discriminants for the four data sets combined, background, and signal for $M_H = 160\,\text{GeV}$ are shown in Fig. 1 . Agreement is observed with expectations from SM background, and the RF-output distributions are therefore used to set upper limits on the cross section for SM Higgs production.
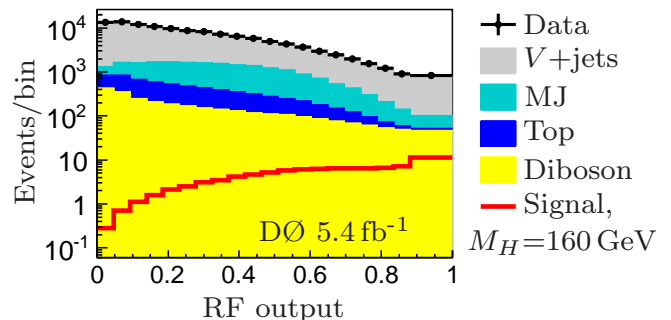

FIG. 1: The output of RF discriminants for data, different backgrounds, and signal for $M_H = 160\,\text{GeV}$ for the combined data sets.

Systematic uncertainties affect the normalizations and distributions of the final discriminants and are included in the determination of limits. These arise from a variety of sources, and their impact is assessed by changing each input discriminant to the RF by ± 1 standard deviation. The most significant uncertainties are from calibration of jet energies (0.7–6)%, jet resolution (0.5–3)%, jet reconstruction efficiency (0.5–4)%, lepton identification and modeling of the trigger (4%), estimation of the multijet background (6.5–26)%, and integrated luminosity (6.1%). Theoretical uncertainties on cross sections for backgrounds are taken from Ref. [20, 23]. The uncertainties on cross sections for signal are taken from Ref. [24]. Because the overall cross section for V+jets production is constrained by data, the uncertainty on its normalization

is anti-correlated with the MJ background. The impacts of theoretical uncertainties on distributions of the final discriminants are assessed by varying a common renormalization and factorization scale, by comparing ALPGEN interfaced with HERWIG [36] to ALPGEN interfaced with PYTHIA for V+jets samples, and by varying PDF parameters using the prescription of Ref. [19] for all MC samples.

Upper limits on the production cross section multiplied by branching fractions are determined using the modified frequentist CL_S approach [37]. A test statistic based on the logarithm of the ratio of likelihoods (LLR) [37] for the data to represent signal+background and background-only hypotheses is summed over all bins of the final discriminant in each set. To minimize degradation in sensitivity, scaling factors for the systematic uncertainties are fitted to the data by maximizing a likelihood function for both the signal+background and background-only hypotheses, with the systematic uncertainties constrained through Gaussian priors on their probabilities [38]. Correlations among systematic uncertainties in signal and background are taken into account in extracting the final results. Figure 2 shows the combined background-subtracted data and the uncertainties on the RF discriminant after they are fitted to the data.
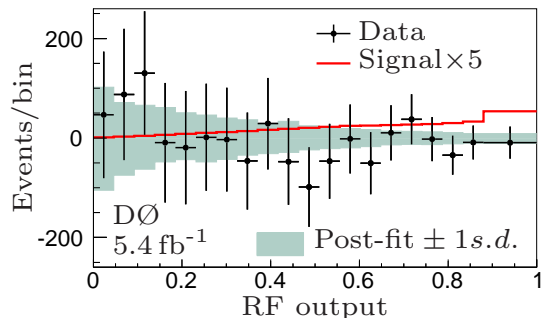

FIG. 2: The combined background subtracted data and one standard deviation (s.d.) uncertainty on total background after applying constraints on systematic uncertainties by fitting to data. The expected SM Higgs signal for $M_H = 160$ GeV, shown by the line, is scaled up by a factor of 5.

The resulting limits on standard model Higgs boson production are given in Table II. The LLR$_{\text{OBS}}$ values shown in Fig. 3 as functions of M_H are within ~ 1.5 standard deviations of the expected median for LLR$_{\text{B}}$, the background-only hypothesis, as calculated from statistical fluctuations and systematic uncertainties.

In conclusion, we have determined the first limits on standard model Higgs boson production examining decays of the Higgs boson to two vector bosons, one of which decays leptonically and the other into a pair of quarks. For $M_H = 160$ GeV, the observed and expected 95% C.L. upper limits on the combined cross section for Higgs production, multiplied by the branching fraction for $H + X \to \ell + \ell/\nu + qq$, are factors of 3.9 and 5.0
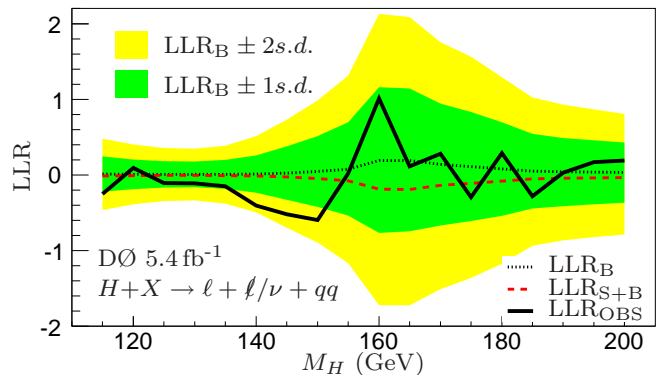

FIG. 3: The observed LLRs for the combined data sets are given by the solid line, the expected LLRs for the background-only and signal+background hypotheses are shown as dots and dashes, respectively, and the dark and light-shaded areas correspond to one and two standard deviations (s.d.) around the expected LLRs for the background-only hypothesis. Negative values of LLR$_{\text{OBS}}$ represent signal-like fluctuations in the data.

larger than the SM cross section, respectively.

Supplementary material, including a list of variables used in the RF, samples of input distributions, and a table of systematic uncertainties, is available from [39].

[1] F. Englert and R. Brout, Phys. Rev. Lett. **13**, 321 (1964).
[2] P. W. Higgs, Phys. Rev. Lett. **13**, 508 (1964).
[3] G. S. Guralnik, C. R. Hagen, and T. W. B. Kibble, Phys. Rev. Lett. **13**, 585 (1964).
[4] P. W. Higgs, Phys. Rev. **145**, 1156 (1966).
[5] V.M. Abazov *et al.* (D0 Collaboration), Phys. Rev. Lett. **104**, 061804 (2010).
[6] T. Aaltonen *et al.* (CDF Collaboration), Phys. Rev. Lett. **104**, 061803 (2010).
[7] T. Aaltonen, *et al.* (CDF and D0 Collaborations), Phys. Rev. Lett. **104**, 061802 (2010).
[8] B. Dobrescu and J. Lykken, J. High Energy Phys. **04**, 083 (2010).
[9] J. F. Gunion and M. Soldate, Phys. Rev. D **34**, 826 (1986).
[10] V.M. Abazov *et al.* (D0 Collaboration), Nucl. Instrum. Methods in Phys. Res. A **565**, 463 (2006); M. Abolins

TABLE II: Ratios of the observed and expected exclusion limits relative to the SM production cross section for $\sigma(p\bar{p} \to H + X)$ multiplied by the branching fraction for $H + X \to \ell + \ell/\nu + qq$ at the 95% C.L. as a function of M_H.

M_H (GeV)	115	120	125	130	135	140	145	150	155	160	165	170	175	180	185	190	195	200
Observed	28.5	20.4	32.8	36.6	33.0	33.7	23.1	17.1	8.3	3.9	5.2	5.6	8.2	7.1	12.0	10.6	10.0	10.4
Expected	19.5	23.4	26.4	28.4	25.7	19.7	13.7	10.4	8.0	5.0	5.1	5.9	6.7	8.0	9.6	10.7	11.2	12.1

et al., Nucl. Instrum. and Methods A **584**, 75 (2007); R. Angstadt et al., Nucl. Instrum. Methods Phys. Res., Sect. A **622**, 298 (2010).

[11] G.C. Blazey et al., arXiv:hep-ex/0005012 (2000).

[12] V.M. Abazov et al. (D0 Collaboration), Phys. Rev. Lett. **101**, 062001 (2008).

[13] T. Andeen et al., FERMILAB-TM-2365 (2007).

[14] M.L. Mangano et al., J. High Energy Phys. **07**, 001 (2003); version 2.11 was used.

[15] V.M. Abazov et al. (D0 Collaboration), Phys. Rev. Lett. **100**, 102002 (2008).

[16] K. Melnikov and F. Petriello, Phys. Rev. D **74**, 114017 (2006).

[17] E. Boos et al. (CompHEP Collaboration), Nucl. Instrum. Methods in Phys. Res. A **534**, 250 (2004).

[18] T. Sjöstrand, S. Mrenna, and P. Skands, J. High Energy Phys. **05**, 026 (2006); version 6.409 with Tune A was used.

[19] J. Pumplin et al., J. High Energy Phys. **07**, 012 (2002); D. Stump et al., J. High Energy Phys **10**, 046 (2003).

[20] J.M. Campbell and R.K. Ellis, Phys. Rev. D **60**, 113006 (1999).

[21] R. Hamberg, W.L. van Neerven, and W.B. Kilgore, Nucl. Phys. B **359**, 343 (1991); **644**, 403(E) (2002).

[22] A.D. Martin, R.G. Roberts, W.J. Stirling, and R.S. Thorne, Phys. Lett. B **604**, 61 (2004).

[23] M. Cacciari et al., J. High Energy Phys. **04**, 068 (2004); N. Kidonakis and R. Vogt, Phys. Rev. D **68**, 114014 (2003); N. Kidonakis, Phys. Rev. D **74**, 114012 (2006).

[24] D. de Florian and M. Grazzini, Phys. Lett. B **674**, 291 (2009); C. Anastasiou, R. Boughezal, and F. Petriello, J. High Energy Phys. **04**, 003 (2009); E.L. Berger and J. Campbell, Phys. Rev. D **70**, 073011 (2004); T. Hahn et al., arXiv:hep-ph/0607308 (2006); M. L. Ciccolini, S. Dittmaier, and M. Krämer, Phys. Rev. D **68**, 073003 (2003); O. Brein, A. Djouadi, and R. Harlander, Phys. Lett. B **579**, 149 (2004); J. Baglio and A. Djouadi, J. High Energy Phys. **10**, 064 (2010); A. Djouadi, J. Kalinowski, and M. Spira, Comput. Phys. Commun. 108, 56 (1998).

[25] S. Frixione and B.R. Webber, J. High Energy Phys. **0206**, 029 (2002).

[26] T. Gleisberg et al., J. High Energy Phys. **02**, 056 (2004).

[27] R. Brun and F. Carminati, CERN Program Library Long Writeup W5013, 1993 (unpublished).

[28] V.M. Abazov et al. (D0 Collaboration), Phys. Rev. D. **76**, 012003 (2007).

[29] The pseudorapidity is defined as $\eta = -\ln[\tan(\theta/2)]$, where θ is the polar angle with respect to the proton beam direction.

[30] V.M. Abazov et al. (D0 Collaboration), Phys. Rev. D. **78**, 012005 (2008).

[31] V.M. Abazov et al. (D0 Collaboration), Phys. Rev. D. **75**, 092007 (2007).

[32] V.M. Abazov et al. (D0 Collaboration), Phys. Rev. Lett. **103**, 141801 (2009).

[33] V.M. Abazov et al. (D0 Collaboration), Phys. Rev. D. **74**, 112004 (2006).

[34] L. Breiman, Machine Learning **45**, 5-32 (2001).

[35] I. Narsky, arXiv:physics/0507143 [physics.data-an] (2005); I. Narsky, arXiv:physics/0507157 [physics.data-an] (2005).

[36] G. Corcella et al., J. High Energy Phys. **01**, 010 (2001).

[37] T. Junk, Nucl. Instrum. Methods in Phys. Res. A **434**, 435 (1999); A. Read, J. Phys. G **28**, 2693 (2002).

[38] W. Fisher, FERMILAB-TM-2386-E.

[39] Supplementary material is provided at http://link.aps.org/supplemental/XX.YYYY/ PhysRevLett.XX.YYYYYY.

Supplementary Material

TABLE III: Variables used in the random forest classifiers, given in categories of object kinematics, angular variables, and event kinematics. The symbol ($\dagger$) denotes a measurement in the rest frame of the reconstructed H boson. A subset of these is used for each channel and data-taking period.

Object Kinematics

Lepton energy	E^ℓ
Lepton/jet transverse momentum	$p_T^\ell, p_T^{j_1}, p_T^{j_2}$

Angular Variables

Azimuthal angles	$\Delta\phi(j_1, j_2), \Delta\phi(\ell, \not{E}_T),$
	$\min[\Delta\phi(\not{E}_T, j_1), \Delta\phi(\not{E}_T, j_2)], \min[\Delta\phi(\ell, j_1), \Delta\phi(\ell, j_2)]$
	$\Delta\phi(\text{bisector of dijet pair}, \not{E}_T)$
Polar angles	$\Delta\eta(j_1, j_2)$
$\eta - \phi$ combinations	$\Delta R(j_1, j_2), \max[\Delta R(\ell, j_1), \Delta R(\ell, j_2)], \min[\Delta R(\not{E}_T, j_1), \Delta R(\not{E}_T, j_2)]$
3D angles	$\text{angle}(j_1, j_2)^\dagger, \text{angle}(j_1, \text{reconstructed } W \to \ell\nu)^\dagger, \text{angle}(\ell, \text{dijet system})$

Event Kinematics

Velocity	$\beta(\text{dijet system})$
Transverse momentum sums	$\not{E}_T, p_T(\text{dijet system}), p_T(\text{leptonic } W)$
	$H_T(j_1, j_2), H_T(\text{all jets}), H_T(j_1, j_2, \ell), H_T(j_1, j_2, \ell, \not{E}_T)$
Topological variables[a]	$\text{aplanarity}(j_1, j_2, \ell, \nu)$
	$\text{centrality}(\ell, j_1, j_2), \text{centrality}(\ell, \text{all jets})$
	$\text{sphericity}(\ell, j_1, j_2), \text{sphericity}(\ell, j_1, j_2, \not{E}_T)$
"N"-body masses	$\text{dijet mass}: M(j_1, j_2), M(j_1, j_2, \ell), M(WW), WW \text{ "visible mass"}: M(j_1, j_2, \ell, \not{E}_T)$
Transverse masses	$M_T(j_1, j_2), M_T(W \to \ell\nu), M_T(WW)$
Ratio of jet energies	$E^{j_2}/E^{j_1\,\dagger}$
$KT^{\mathrm{max/min}}$	$\Delta R(j_1, j_2) \cdot E_T(j_{1/2})/(E_T^\ell + \not{E}_T)$
Other combinations	scalar product of $\not{E}_T$ and angular bisector of dijet pair
	$\Delta\phi(W^\ell, \text{bisector of dijet system})$
	Magnitude of $p_T^{j_1}$ perpendicular to dijet system
Scaled $\not{E}_T$	$\displaystyle\sum_{\text{all jets}} [\sqrt{E^{j_i}} \sin(\theta^{j_i}) \cos(\Delta\phi(j_i, \not{E}_T))]^2$

[a]For descriptions of the topological variables see: V.D. Barger and R.J.N. Phillips, Collider Physics, Addison-Wesley, Reading, MA, 1987.
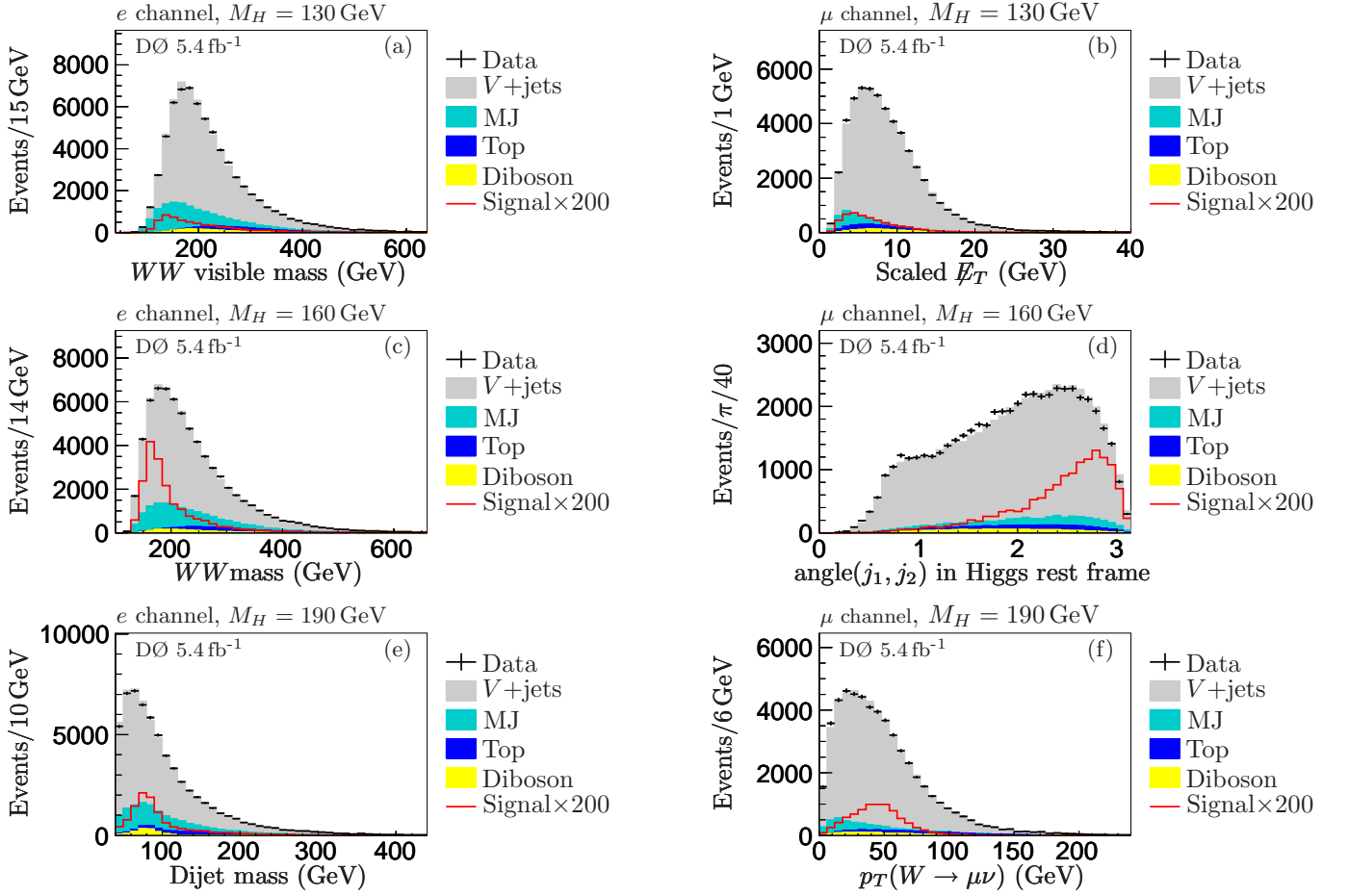
FIG. 4: Sample of DT inputs for (a,c,e) electron and (b,d,f) muon channels. The data are shown as points with uncertainties. The background contributions are shown as histograms, with sources indicated in the legend. "V+jets" includes $(W/Z)+(u, d, s, c, b, g)$ jets, MJ is the multijet background, "top" includes pair and single top quark production, diboson includes WW, WZ, and ZZ processes. The distributions for signal are multiplied by a factor of 200.

TABLE IV: Systematic uncertainties for the electron and muon channels. Signal uncertainties are shown for $M_H = 160\,\mathrm{GeV}$ for all channels except for WH, shown for $M_H = 115\,\mathrm{GeV}$. Those affecting the shape of the RF discriminant are indicated with "Y." Uncertainties are listed as relative changes in normalization, in percent, except for those also marked by "S," where the the overall normalization is constant, and the value given denotes the maximum percentage change from nominal in any region of the distribution.

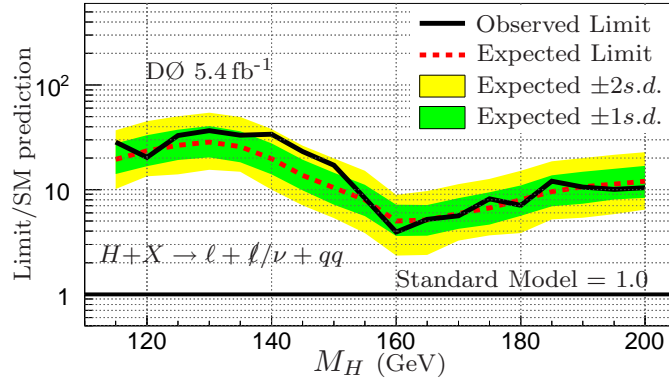| Contribution	Shape	W+jets	Z+jets	top	diboson	$gg \to H$	$qq \to qqH$	WH
Jet energy scale	Y	$\left(^{+6.7}_{-5.4}\right)^S$	< 0.1	± 0.7	± 3.3	$\left(^{+5.7}_{-4.0}\right)$	± 1.5	$\left(^{+2.7}_{-2.3}\right)$
Jet identification	Y	$\pm 6.6^S$	< 0.1	± 0.5	± 3.8	± 1.0	± 1.1	± 1.0
Jet resolution	Y	$\left(^{+6.6}_{-4.1}\right)^S$	< 0.1	± 0.5	$\left(^{+1.0}_{-0.5}\right)$	$\left(^{+3.0}_{-0.5}\right)$	± 0.8	± 1.0
Association of jets with PV	Y	$\pm 3.2^S$	$\pm 1.3^S$	± 1.2	± 3.2	± 2.9	± 2.4	$\left(^{+0.9}_{-0.2}\right)$
Luminosity	N	n/a	n/a	± 6.1	± 6.1	± 6.1	± 6.1	± 6.1
Muon trigger	Y	$\pm 0.4^S$	< 0.1	< 0.1	< 0.1	< 0.1	< 0.1	< 0.1
Electron identification	N	± 4.0	± 4.0	± 4.0	± 4.0	± 4.0	± 4.0	± 4.0
Muon identification	N	± 4.0	± 4.0	± 4.0	± 4.0	± 4.0	± 4.0	± 4.0
ALPGEN tuning	Y	$\pm 1.1^S$	$\pm 0.3^S$	n/a	n/a	n/a	n/a	n/a
Cross Section	N	± 6	± 6	± 10	± 7	± 10	± 10	± 6
Heavy-flavor fraction	Y	± 20	± 20	n/a	n/a	n/a	n/a	n/a
PDF	Y	$\pm 2.0^S$	$\pm 0.7^S$	$< 0.1^S$	$< 0.1^S$	$< 0.1^S$	$< 0.1^S$	$< 0.1^S$
		Electron channel			Muon channel			
Multijet Background	Y	± 6.5			± 26			

FIG. 5: Ratio of the 95% CL limit to the SM expectation as a function of M_H for the electron and muon channels combined. Expected limits are shown by the dashed line, observed limits are shown by the solid line. The heavy and light shaded areas correspond to one and two standard deviations (s.d.) around the expected result for the background-only hypothesis.